ChalcogenideLetters Vol. 7, No. 11, November 2010, p. 631-640

ON THE PREPARATION OF MANGANESE-DOPED ZINC SULPHIDE NANOCRYSTALLINE POWDERS USING THE WET- CHEMICAL SYNTHESIS ROUTE

A.-I. CADIŞ[a], E.-J. POPOVICI[a*], E. BICA[a], I. PERHAIŢĂ[a],
L. BARBU-TUDORAN[b], E. INDREA[c],
[a]*"Raluca Ripan" Institute for Research in Chemistry, "Babes- Bolyai" University, Fântânele Str. no. 30, 400294 Cluj-Napoca, ROMANIA*
[b] *Electronic Microscopy Centre, "Babes-Bolyai" University, Clinicilor Str. No 5-7, 400006 Cluj-Napoca, ROMANIA*
[c]*National Institute for Research and Development of Isotopic and Molecular Technologies, Donath Str. No 65-103, 400293 Cluj-Napoca, ROMANIA*

Manganese-doped zinc sulphide nanocrystalline powders were synthesised by precipitation from Zn-Mn acetate and sodium sulphide, using the reagent sequential addition *SeqAdd* technique. Precipitation was carried out at low temperatures (5°C), from an aqueous medium, containing different Mn^{2+} amounts and various organic reagents, in order to control both the morpho-structural and optical properties of ZnS:Mn^{2+} particles. All samples were characterized by ICP-optical emission spectroscopy, thermal analysis, infrared absorption spectroscopy, photoluminescence emission and excitation spectroscopy, transmission electron microscopy and X-ray diffraction. A correlation between the preparation conditions and the physical-chemical properties, photoluminescence and morpho-structural characteristics of ZnS:Mn^{2+}powders was established.

(Received October 28, 2010; accepted November 27, 2010)

Keywords: Mn-doped ZnS; nanoparticles; photoluminescence; precipitation;

1. Introduction

Semiconductor nanoparticles have been extensively studied from experimental and theoretical viewpoints, owing to their potential applications, consequent to their size-dependent optical properties. Among all semiconductor nanoparticles, zinc sulphide (ZnS) is an interesting material with many applications in various fields such as optoelectronics [1], photocatalysis [2], solar energy conversion [3], projection television [4], fluorescence microscopy [5] etc.

New properties and applications have been obtained through controlling the size and the doping of ZnS particles with transition metal ions [6] or rare-earth ions [7]. Manganese-doped zinc sulphide ZnS:Mn^{2+} nanocrystals could exhibit orange luminescence with high fluorescence quantum efficiency under the interband excitation of the host crystal by UV light [8]. This spectacular result suggested that nanocrystalline ZnS:Mn^{2+} systems may form a new class of luminescent material with applications to displays, lighting and lasers [9].

The increasing interest in ZnS nanoparticles (NPs) has lead to the development of a variety of chemical synthesis routes including ultrasound irradiation [10], microwave irradiation [11], sol–gel method [12], electrochemical template synthesis [13], solid-state reaction [7], gas-phase condensation [14], chemical precipitation [15], and microemulsion with hydrothermal treatment [16]. From all these works, it has been found that particle size and luminescent properties of ZnS powders depend strongly on the specific preparation method and the applied experimental conditions. The most popular method for the precipitation of luminescent zinc

sulphide is the wet-chemical synthesis -*WCS* route that allows the use of cheap raw materials and has a large-scale-production potential [17].

As revealed by our previous studies regarding the synthesis of luminescent materials, WCS route can be performed using two different precipitation techniques namely the reagent sequential addition *SeqAdd* and the reagent simultaneous addition *SimAdd* [18, 19].

According to the literature [20-22], the preparation of ZnS nanoparticles by *WCS* route is usually performed with the *SeqAdd* precipitation technique and the particle growth is controlled with appropriate amounts of organic reagents that act as surfactants i.e. mercaptoethanol, cysteine, hexadecyltrimethyl ammonium bromide, sodium dodecylsulphate [23] or as passivating agents i.e. poly (methyl methacrylate), 3-methacryloxypropyl trimethoxysilane, methacrylic acid [23].

In order to develop new preparation routes or/and new chalcogenide-based materials with luminescent properties, we focused our attention toward the synthesis and characterisation of luminescent zinc sulphide nanostructured layers and nanoparticles [10, 15, 25, 26]. In this paper, some physical-chemical aspects referring to the *WCS* preparation of manganese doped ZnS nanocrystalline powders, using the reagent sequential addition technique-*SeqAdd* are reported. In order to control the particle morphology and size, two organic additives were used namely methacrylic acid MAA and sodium dodecylsulphate SDS as passivating and tensioactive agents, respectively. Our investigation was focussed on the influence of Mn-concentration as well as of the organic reagents on the photoluminescence and morpho-structural properties of ZnS:Mn^{2+} powders.

2. Experimental

Zinc sulphide-based powders were prepared by wet chemical synthesis route, using the reagents sequential addition technique SeqAdd. Precipitation of ZnS:Mn^{2+} powders was carried out at low temperatures (5°C), in aqueous medium, from 1M aqueous solutions of Zn-Mn acetate and sodium sulphide, respectively. In this purpose 50 ml of Zn-Mn acetate solution (1M) prepared from $Zn(CH_3COO)_2$and $Mn(CH_3COO)_2$ stock solutions was added into 400 ml deionised water containing 20.3 g/l. organic reagent i.e. methacrylic acid – MAA or sodium dodecylsulphate – SDS. 50 ml of 1M aqueous solution of Na_2S was added to the above mixture solution and vigorously stirred for 30 min. The resulting ZnS:Mn^{2+} powders were cautiously washed with deionised water and isopropyl alcohol, centrifuged, and finally dried at 80°C, under vacuum. $Zn(CH_3COO)_2$ and Na_2S stock solutions were previously purified by cross-precipitation.

The infrared absorption spectra (FT-IR) of ZnS:Mn^{2+} samples were registered on a THERMO SCIENTIFIC NICOLET™ 6700 FT-IR spectrometer (KBr pellets). *Photoluminescence emission (PL) and photoluminescence excitation (PLE) spectra* were registered with JASCO FP-6500 spectrofluorimeter Wavell (PMT R928 photomultiplier; glass filter WG 320-ReichmannFeinoptik). The most intense sample (C75) was used as internal standard (I_{em}=100%). *The thermogravimetric analysis (TGA)* was performed with a METTLER-TOLEDO TGA/SDTA851 instrument (nitrogen flow; 5°C/min heating rate; 150 or 900 µl alumina crucibles). *The transmission electron microscopy (TEM)* was performed with JEM JEOL 1010 microscope (accelerating voltage of 20 kV). *X-Ray diffraction (XRD*) patterns were recorded using D8 ADVANCED BRUKER diffractometer (CuKα radiation; Ni filter; alumina/corundum powder as standard for instrument broadening correction). The amount of manganese and zinc in ZnS:Mn^{2+} powders was determined by inductively coupled plasma optical emission spectroscopy ICP-OES using a PERKIN ELMER OPTIMA 2100 DV spectrometer (0.1 g powder digested in 50 ml HCl solution).

3. Results and discussion

The goal of our study was to obtain luminescent manganese doped zinc sulphide nanocrystals using the *SeqAdd* precipitation technique. In this respect, attempts were made to prepare ZnS:Mn^{2+} nanoparticles with variable manganese amounts, in the presence of organic

reagents i.e. methacrylic acid – MAA as passivating agents or sodium dodecylsulphate – SDS as ionic surfactant.

The as obtained powders are double metallic sulphides (1-x)ZnS·xMnS type, and their formation takes place by the simultaneous precipitation of zinc sulphide and manganese sulphide, as described by the following overall equation:

$$(1\text{-}x)Zn(CH_3COO)_2 + xMn(CH_3COO)_2 + Na_2S \rightarrow (1\text{-}x)ZnS{\cdot}xMnS + 2CH_3COONa$$

Two samples series were precipitated from an aqueous medium with the same organic reagent MAA and variable manganese amounts i.e. 0 mol % (C17), 5.6 mol % (C19), 11.0 mol % (C73), 16.4 mol % (C21) and 25.0 mol % (C77) and, correspondingly, with the same manganese amount 16.4 mol% and different organic reagent i.e. MAA (C21), no additive (C74) and SDS (C75); manganese amount was estimated in relation with the total amount of Zn and Mn, from the precipitation medium.

The influence of both the manganese concentration and organic reagents on the general physical- chemical, luminescent and morpho-structural properties of $ZnS:Mn^{2+}$ powders was investigated.

3. 1. Physical-chemical properties

The manganese concentration in $ZnS:Mn^{2+}$ powders is much lower than the theoretical values, as revealed by ICP-OES data. Moreover, the fine dispersed ZnS-based powders show a high capacity to absorb anionic impurities from the precipitation medium, as illustrated by the thermal analysis and the FT-IR spectroscopy. Table 1 presents the Mn/(Mn+Zn) ratio used in the synthesis and determined by ICP-OES investigation as well as the main thermogravimetric data of samples obtained in different conditions.

The manganese concentration in ZnS powders is under 5% from the theoretical value. This can be explained by the fact that, the precipitation rate of the two metallic sulphides is unequal, due to the large difference between the solubility product of zinc sulphide, namely 2.5×10^{-22} for cubic ZnS form, and manganese sulphide, namely 2.5×10^{-10} for amorphous MnS form. As a result, the manganese concentration in $ZnS:Mn^{2+}$ powders is much lower than the theoretical value.

Table 1. ICP-OES and TGA analysis data for $ZnS:Mn^{2+}$ powders obtained in different precipitation conditions.

Code	Organic reagent	ICP analysis (mol%) Mn*100/ (Mn+Zn)			Thermal analysis data			
					Weight-loss (wt%)			Sublimation point
		used in synthesis	determined	co-precipitated	20-200°C	200-900°C	900-1050°C	
C17	MAA	0.0	0.00	0.00 %	-7.4	-13.0	-3.8	1042
C19	MAA	5.6	0.07	1.25 %	-10.6	-13.0	-3.6	1011
C73	MAA	11.0	0.18	1.64 %	-6.4	-8.5	-4.0	1034
C21	MAA	16.4	0.22	1.34 %	-7.5	-12.5	-3.8	1021
C77	MAA	25.0	0.45	1.80 %	-7.5	-9.7	-4.0	1043
C21	MAA	16.4	0.22	1.34 %	-6.1	-16.1	-2.0	1035*
C74	-	16.4	0.67	4.09 %	-5.4	-9.6	-2.4	1040*
C75	SDS	16.4	0.71	4.33 %	-6.1	-19.3	-2.9	1037*

*TGA performed with double amount of sample, in relative large crucibles

The study revealed that, the Mn amount incorporated into ZnS nanocrystals is very dependent on the organic reagent used as particle size regulator. The co-precipitation level is of about 4.0-4.5 % for samples obtained with no additive or with SDS, and only of 1-2% in samples prepared with the passivating agent. It is obvious that the MAA addition decreases the precipitation rate of MnS in comparison with ZnS.

The thermal behaviour of $ZnS:Mn^{2+}$ powders is dependent on the precipitation conditions (Table 1). All samples show three major endothermic stages that can be associated with: a)

removal of physical adsorbed or loosely bound water (under about 200°C); b) removal of organic ionic species adsorbed from the precipitation medium (between about 200 and 900°C); c) ZnS volatilization under the cumulative effect of temperature and nitrogen flow (between 900°C and 1050°C). The volatilization/ sublimation level expressed by the weight-loss in 900-1050°C domain is dependent on the ZnS:Mn^{2+} powder dispersions and particle dimensions. The sublimation point was estimated through the onset temperature, after 900°C, on the TGA curves.

For samples prepared with MAA and variable Mn-amounts, the weight-loss values are similar (excepting samples C19). They correspond to a water amount of 6.5-7.5%, an organic impurity content of 8.5 – 13.0 % (relative higher for a lower Mn co-precipitation level) and a sublimation level of 3.6 - 4 %. Instead, for samples prepared with /without organic reagent the weight-loss values are different. In this case, sample prepared with SDS (C75) have the highest organic impurity level (19.3%) and the highest sublimation level (2.9%) as compared with no-additive or MAA-sample. The powder obtained with MAA (C21) shows low powder dispersion, as suggested by the lowest sublimation level (2%).

The influence of the organic additive on the thermogravimetric (TG) and differential thermogravimetric (DTG) curves is illustrated in Figure 1. One can note that in the temperature range 200-900 °C related to the organics removal, the weight-loss takes place in: a) two steps (C74) for the decomposition of the adsorbed acetate; b) three steps (C21) for acetate and MAA decomposition and c) four steps (C75) for acetate and SDS thermal dissociation, including the SO_2 emission.

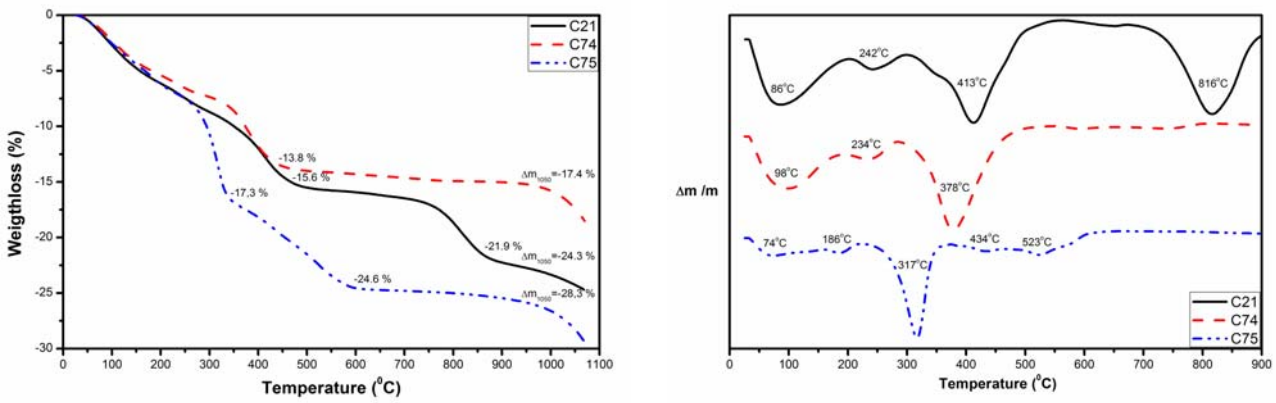

Fig. 1. TG (left) and DTG (right) curves of samples prepared with various organic reagents MAA (C21), C74 (no additive) and C75 (SDS)

The organic impurities absorbed on the surface of ZnS:Mn^{2+} particles are put in evidence by the infrared spectroscopy (Figure 2). For comparison, the vibrational spectrum of the calcined ZnS:Mn^{2+} sample is depicted in the inset graph.

Besides the broad and weak band at about 480 cm^{-1} assigned to Zn-S bond, FT-IR spectra show the characteristic vibration bands for water, acetate and multi-atomic ions adsorbed from the precipitation medium. The most important absorption bands for ZnS:Mn^{2+} powder obtained without additive (C74) are situated between 1300 and 1600 cm^{-1} and they are assigned to H_2O and COO groups from acetate ion (CH_3COO^-). FT-IR spectra of samples obtained with MAA (C21) and SDS (C75) contain some additional absorption bands in the 1000-1200 cm^{-1} domain, assigned to C=C and =CH bonds of methacrylate ion (CH_2=C(CH_3)-CO-O^-), or in the 950-1100; 2800-3000 cm^{-1} and 1100-1300 cm^{-1} range, corresponding to CH_3 and SO_2 groups, respectively, in relation with dodecylsulphate ion ($CH_3(CH_2)_{11}O$-SO_2-O^-) [27].

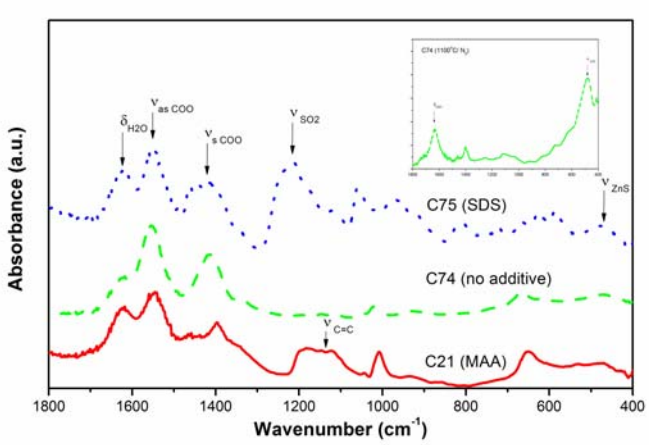

Fig. 2. FT-IR spectra of ZnS:Mn^{2+} samples prepared with/without organic reagents (normalised)

FT-IR and TGA investigations revealed the high capacity of ZnS:Mn powders to absorbs anionic species from the precipitation medium, thus illustrating their large surface area in correlation with the small particle dimensions.

3.2. Photoluminescence properties

Under ultraviolet excitation, all manganese doped ZnS powders show orange luminescence with variable brightness, function of the synthesis conditions. The photoluminescence emission spectra (PL) are depicted in Figure 3. The un-activated sample (C17) exhibits only a weak blue emission band (about 435 nm) attributed to the defect-related emission of the ZnS host. For Mn^{2+}doped samples, a second emission band centred at about 600 nm is observed, as expected. The characteristic orange emission, which has been observed in different Mn-doped semiconductors, is associated with $^4T_1$–$^6A_1$ electronic transitions inside the manganese ion [28].

Figure 4 shows the photoluminescence excitation (PLE) spectra for the Mn^{2+} emission in samples with different doping levels. As expected, the two possible excitation paths from doped semiconductors are put in evidence namely, the indirect one that includes the host lattice and the direct one that implies the doping ions. The maximum excitation peak of Mn^{2+} emission centred at about 340 nm is related with the fundamental absorption of the ZnS host whereas the relative smaller spectral peaks in the 375-575 nm domain arise from the direct excitation transitions of Mn^{2+}. In this domain, PLE intensity increases with Mn concentration. According to the literature [29], these absorption peaks observed in Mn^{2+} bands at about 390, 430, 465, 500, and 535 nm are attributed to the transitions between the $^6A_1(^6S)$ ground state and the excited states of $^4E(^4D)$, $^4T_2(^4D)$, $^4A_1(^4G)$ and $^4E(^4G)$, $^4T_2(^4G)$, $^4T_1(^4G)$ within the Mn^{2+} $3d^5$ configuration, respectively.

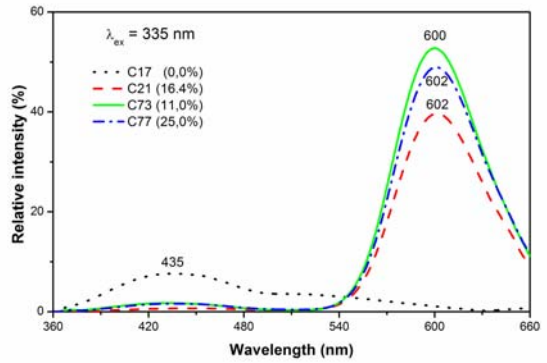

Fig. 3. PL spectra of ZnS:Mn^{2+} powders prepared with MAA and various Mn^{2+} amounts

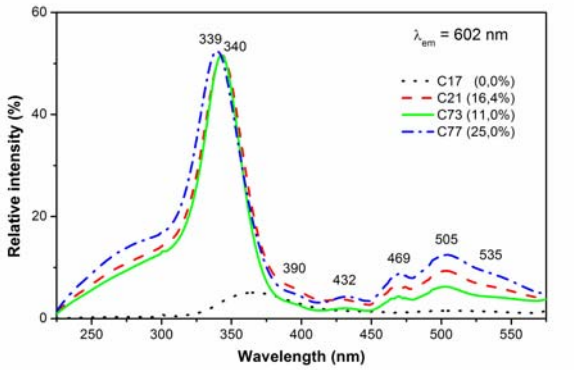

Fig. 4. PLE spectra of ZnS:Mn^{2+} powders prepared with MAA and various Mn^{2+} amounts

The relative intensity of the blue and orange band emissions is plotted as a function of the manganese amount Mn *100/(Mn+Zn), as determined by ICP-OES analysis (Figure 5). The sample without Mn^{2+} shows only the ZnS-related blue photoluminescence. As soon as Mn^{2+} is incorporated into the ZnS crystals, the intensity of the blue emission decreases and the Mn^{2+} emission comes up, since the energy transfer between ZnS host and Mn^{2+} impurity is very efficient. The luminescence intensity of the orange band increases in parallel with Mn^{2+} concentration and then decreases. The maximum of intensity value is reached at about 0.18% Mn^{2+} and it corresponds to the optimum ratio between the number of the emission centres and the quenching ones. The irregular variation of the emission intensity with Mn-amount indicates that PL performance is influenced not only by the doping level, but also by other factors including surface state and crystalline order degree of un-annealed ZnS powders.

The blue band intensity decreases continuously with the increase of Mn^{2+} amount, due to the decrease of the numbers of self activated centres related with the lattice defects of the zinc sulphide.

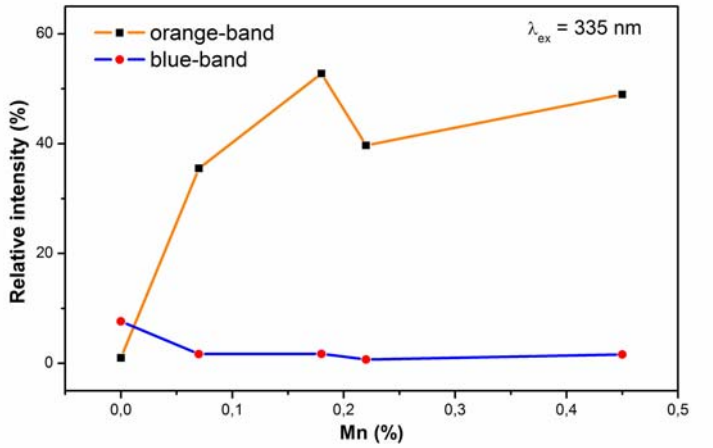

Fig. 5. Relative intensity of the orange and blue bands versus the incorporated Mn amount (MAA-samples)

PL and PLE spectra of ZnS:Mn^{2+} powders precipitated from a medium with identical Mn-concentration (16.4 mol% used in the synthesis) and with various organic reagents are shown in Figure 6 and Figure 7, respectively.

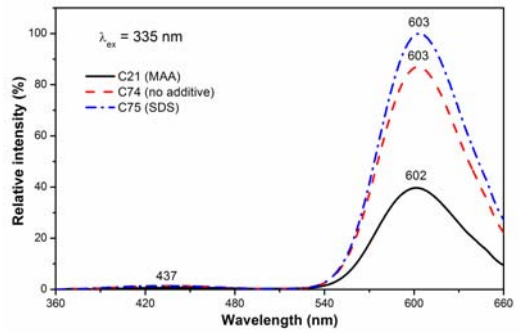

Fig. 6. PL spectra of ZnS:Mn^{2+} powders prepared with/without organic reagents

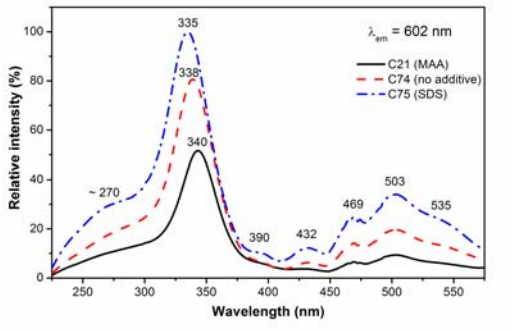

Fig. 7. PLE spectra of ZnS:Mn^{2+} powders prepared with/without organic reagents

The addition of SDS increases the intensity of the orange emission with about 15% whereas the MAA decreases it with about 20%, in comparison with the no-additive sample. This effect seems to be related with the real amount of Mn-incorporated into ZnS-crystals i.e. 0.67% (no-additive samples), 0.22% (MAA-sample) and 0.71 (SDS- sample).

PLE spectra reveal the direct and indirect excitation paths in ZnS:Mn^{2+} powders. The position and the intensity of the UV-excitation band (indirect path) associated with the ZnS

fundamental absorption is strongly influenced by the organic reagent. This suggests that the luminescence performance of ZnS:Mn^{2+} samples is determined not only by the amount of Mn^{2+} incorporated into the host crystals, but also by the organic additive adsorbed on the surface of particles. One can presume that the adsorbed SDS acts as molecular sensitizer for Mn-emission whereas the adsorbed MAA behaves as a molecular quencher.

3.3.Morpho-structural properties

Figure 8 shows the transmission electron microscopy (TEM) images of the powders obtained with/ without organic reagent (C21, C74, C75). They illustrate that ZnS:Mn^{2+} powders consists from very small particles with diameters under 10 nm, showing a strong tendency toward agglomeration, due to their large surface area.

TEM investigations put also in evidence that the organic reagents slow down the particle growth, the effect being relatively stronger for MAA than SDS.

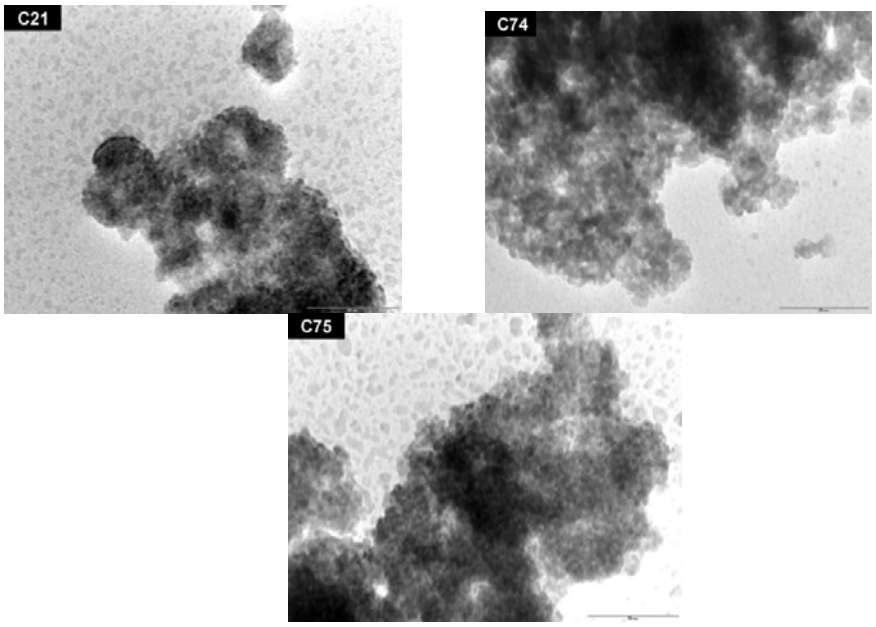

Fig. 8. TEM images of Mn-doped ZnS powders prepared with/without organic reagents: C21 (MAA); C74 (no additive); C75 (SDS); scale bar = 50 nm.

XRD patterns of ZnS powders were interpreted using ITO12 from the CRYSFIRE set [30] whereas the unit cell parameters were calculated by Rietveld refinement, using the POWDERCELL software [31]. They indicate the formation of a single phase, nanocrystalline material with pure ZnS cubic phase, whatever the synthesis conditions. Figure 9 illustrates the three specific diffraction peaks originating from (111), (220) and (311) planes of the zinc blende structure (PDF 65-0309).

Relevant information was provided by the microstructural parameters obtained by X-ray profile Fourier analysis. In this respect, the single [111], [220] and [311] profiles, at 2Θ = 28.54; 47.46 and 56.32 degrees, respectively, were analysed by Warren-Averbach method and processed by XRLINE program [32-34]. The analysis was performed for ZnS-cubic system (PDF 65-0309; G.S. 216; unit cell parameters: a=b=c=0.540 nm; V= 0.1574 nm^3).

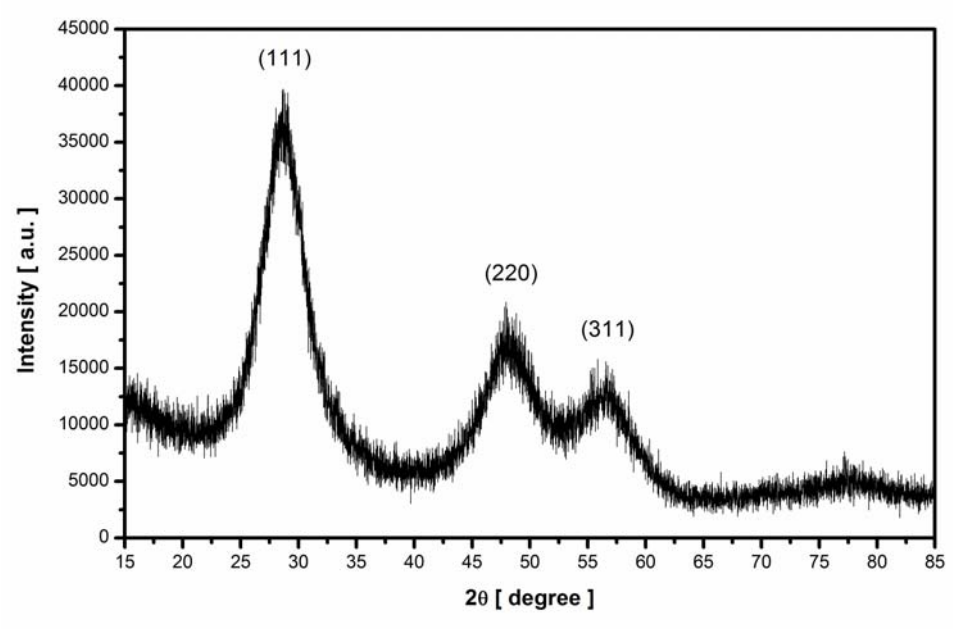

Fig. 9. XRD pattern of un-doped ZnS sample (C17)

The effective crystallite mean size (D_{eff}) and the root mean square (r.m.s.) of the microstrains $<\varepsilon^2>^{1/2}$hkl averaged along the [hkl] direction were determined. The XRD microstructural data as well as some of the sample characteristics are presented in table 2.

Table 2. Unit cell parameters of some ZnS:Mn^{2+} powders and their relevant characteristics.

Samples	Synthesis details		PL	Structural data			
	Organic reagent	Mn concn. [mol%]	Intensity [%]	a=b=c [nm]	V [nm^3]	D_{eff} [nm]	$<\varepsilon^2>^{1/2}_m$ x 10^2
C17	MAA	0.00	1	0.5414	0.15869	2.96	0.9457
C21	MAA	0.22	40	0.5415	0.15883	3.20	1.0408
C77	MAA	0.45	49	0.5417	0.15899	2.96	0.9469
C74	-	0.67	84	0.5422	0.15919	2.96	0.9469
C75	SDS	0.71	100	0.5416	0.15882	2.96	0.9459

Micro-structural parameters i.e. the effective crystallite mean size and the root mean square of the microstrains illustrate that, in our experimental conditions, all ZnS powders are composed from nanoparticles (D_{eff} ≈3 nm), with an intermediate density of packing defects (r.m.s.≈ 0.01). The crystallite size seems to be independent of both, the Mn-concentration and the organic reagent presence.

The unit cell parameters of ZnS:Mn^{2+} powders are in agreement with the theoretical values. The cell volume indicates that the crystalline lattice of nanocrystals obtained with MAA and SDS are relatively strongly packed as compared with powders obtained without organic reagent. On the other hand, the unit cell volume slightly increases with Mn-concentration. This is an expected tendency if one consider that, in zinc sulphide lattice, 0.074 nm Zn^{2+} ions are substituted with 0.080 nm Mn^{2+} ions (tetrahedral coordination).

One can also note that, the high PL intensity of sample C75 can be justified by the relatively high amount of Mn^{2+} incorporated into a less deformed crystalline lattice.

4. Conclusions

Manganese-doped zinc sulphide powders were prepared by *WCS* route, using the reagent sequential addition technique *SeqAdd* of precipitation. WCS conditions i.e. low precipitation temperature, organic additives and variable manganese amount, enabled us to obtain relatively strong luminescent ZnS:Mn^{2+} nanocrystals.

The organic additives, either tensioactive or passivating agents, show similar effect on the morpho-structural properties, but they exhibit different impact on the photoluminescence performances, in relation with both the Mn-doping level (1.3- 4.3 % from the theoretical amount) and the organic impurities adsorbed on the particle surface.

The highest PL performance, associated with the optimum ratio between the number of the emission centres and the quenching ones, is obtained for ZnS:Mn powders prepared from an aqueous medium with SDS as additive and 16.4 mol% Mn, factors that allow the highest incorporation of Mn^{2+}ions (~ 0.7%). One can presume that the adsorbed SDS acts as molecular sensitizer for Mn-emission whereas the adsorbed MAA behaves as a molecular quencher.

XRD investigation indicate the formation of a single phase nanocrystalline material (cubic ZnS), whatever the synthesis conditions. The effective crystallite mean size is about 3 nm and the packing density of defects has an intermediate value (r.m.s.~ 0.01). The strong orange photoluminescence of the un-annealed ZnS:Mn^{2+} powders obtained in our experimental conditions can be associated with the particle nano-dimension and the consequent PL confinement.

In order to obtain ZnS:Mn nanocrystalline powders with superior PL performances, other experimental studies based on *SimAdd* technique of precipitation are to be performed in the near future.

Acknowledgments

This work was supported by CNCSIS –UEFISCSU, project number PNII – IDEI 2488/2008.

References

[1] X. J. Zheng, Y. Q. Chen, T. Zhang, C. B. Jiang, B. Yang, B. Yuan, S. X. Mao, W. Li, Scripta. Mater. **62**, 520 (2010).
[2] C. Unni, D. Philip, K. G. Gopchandran, Opt. Mater. **32**, 169 (2009).
[3] J. S. Jang, C. J. Yu, S. H. Choi, S. M. Ji, E. S. Kim, J. S. Lee, J. Catal. **254**, 144 (2008).
[4] J. F. Suyver, S. F. Wuister, J. J. Kelly, A. Meijerink, Nano Lett. **1**, 429 (2001).
[5] D. Yelin, D. Oron, S. Thiberge, E. Moses, Y. Silberberg, Opt. Express. **11**, 1385 (2003).
[6] B. Steitz, Y. Axmann, H. Hofmann, A. Petri-Fink, J. Lumin. **128**, 92 (2008).
[7] L. P. Wang, X. D. Xu, X. Yuan, J. Lumin. **130**, 137 (2010).
[8] R. N. Bhargava, D. Gallagher, X. Hong, A. Nurmikko, Phys. Rev. Lett. **72**, 416 (1994).
[9] A. A. Bol, A. Meijerink, J. Lumin. **87-89**, 315 (2000).
[10] A.-R. Tomsa, E.-J. Popovici, A.-I. Cadis, M. Stefan, L. Barbu-Tudoran, S. Astilean, J. Optoelectron. Adv. Mater. **10**, 2342 (2008).
[11] J. Q. Sun, X. P. Shen, K. M. Chen, Q. Liu, W. Liu, Solid. State Commun. **147**, 501 (2008).
[12] M. M. Biggs, O. M. Ntwaeaborwa, J. J. Terblans, H. C. Swart, Physica B **404**, 4470 (2009).
[13] Z. Jindal, N.K. Verma, J. Optoelectron. Adv. Mater. **10**, 3283 (2008).
[14] J. C. Sanchez-Lopez, A. Justo, A. Fernandez, Langmuir **15**, 7822 (1999).
[15] A.-I. Cadis, A.-R. Tomsa, M. Stefan, R. Grecu, L. Barbu-Tudoran, L. Silaghi-Dumitrescu, E.-J. Popovici, J. Optoelectron. Adv. Mater. - Symposia **2**, 111 (2010).
[16] S. J. Xu, S. J. Chua, B. Liu, L. M. Gan, C. H. Chew, G. Q. Xu, Appl. Phys. Lett. **73**, 478 (1998).

[17] Z. L. Wang, Y. Liu, Z. Zhang, Handbook of Nanophase and Nanostructured Materials Synthesis, Tsinghua University Press and Kluwer Academic Plenum Publishers, New York (2002)
[18] L. Muresan, E.-J. Popovici, R. Grecu, L. Barbu Tudoran, J. Alloys Compd. 471, 421 (2009).
[19] E-J. Popovici, M. Morar, L. Mureşan, R. Grecu, L. Barbu-Tudorana, E. Indrea, J. Optoelectron. Adv. Mater.-Symposia 1, 1000 (2009).
[20] B. Bahmani, F. Moztarzadeh, M. Rabiee, J. Optoelectron. Adv. Mater. **9**, 3336 (2008).
[21] G. Murugadoss, B. Rajamannan, U. Madhusudhanan, Chalcogenide Lett. **6**, 197 (2009).
[22] S. Chellammal, S. Sankar, S. Selvakumar, E. Viswanathan, R. Murugaraj, K. Sivaji, J. Mater. Sci. **45**, 1242 (2010).
[23] R. Thiruvengadathan, Y. Levi-Kalisman, O. Regev, Ultrason. Sonochem. 14, 398 (2007)
[24] W.Q. Peng, S.C.; Qu, G.W. Cong, X.Q. Zhang, Z.G. Wang, J. Cryst. Growth. 282, 179 (2005)
[25] M. Stefan, I. Baldea, R. Grecu, E. Indrea, E.-J. Popovici, Studia Universitatis Babes-Bolyai Chemia **54**, 203 (2009).
[26] A.-I. Cadis, E.-J. Popovici, E. Bica, I. Perhaita, L. Barbu-Tudoran, E. Indrea, IEEE Proceeding of "The 33rd International Semiconductor Conference CAS2010 , Sinaia, Romania (in press).
[27] B. H. Stuart, Infrared Spectroscopy: Fundamentals and Applications, John Wiley & Sons Ltd., Chichester (2004).
[28] R. Kripal, A.K. Gupta, S.K. Mishra, R.K. Srivastava, A.C. Pandey, S.G. Prakash, Spectrochim. Acta, Part A 76, 523 (2010).
[29] W. Q. Peng, S. C. Qu, G. W. Cong, X. Q. Zhang, Z. G. Wang, J. Cryst. Growth. **282**, 179 (2005).
[30] W. Kraus, G. Nolze, J. Appl. Crystallogr. **29**, 301 (1996).
[31] J. W. Visser, J. Appl. Cryst. **2**, 89 (1969).
[32] J. G. M. van Bercum, A. C. Vermeulen, R. Delhez, T. H. de Keijser, E. M. Mittemeijer, J. Appl. Phys., **27**, 345 (1994).
[33] E. Indrea, A. Barbu, Appl. Surf. Sci., **106**, 498 (1996).
[34] N. Aldea, E. Indrea, Comput. Phys. Commun., **60**, 155 (1990).